Microstructures and Mechanical Properties of Non-thinning and Penetrating Friction Stir Welded 2219-T6 Aluminum Alloy

Dongrui Li
Huijie Liu (liuhj@hit.edu.cn)
Harbin Institute of Technology https://orcid.org/0000-0003-4821-5986
Siping Chen
Shuaishuai Du
Yanying Hu
Xuanmo Li
Yisong Gao

Research Article

Keywords: Non-thinning friction stir welding, Penetrating friction stir welding, Archimedes spiral groove, Microstructure, Mechanical properties

Posted Date: March 7th, 2022

DOI: https://doi.org/10.21203/rs.3.rs-1407265/v1

Abstract

In the conventional friction stir welding (CFSW) process, a certain size spindle tilting angle and shoulder plunge depth were applied in order to obtain high-quality welds. However, what was the reason for the thinning phenomenon of weld and thus the weakening of weld bearing capacity? The reduction of spindle tilting angle and shoulder plunge depth was likely to cause the welding tool not being able to reach the weld root, and thus it was engendered for the kissing bond or the absence of complete penetration. In the present study, a novel welding tool with large-size shoulder and Archimedes spiral groove was designed in order to achieve non-thinning and lack of kissing bond welds. The microstructures and mechanical properties of the joints obtained by the Non-thinning and Penetrating Friction Stir Welding (NTPFSW) and the Penetrating Friction Stir Welding (PFSW) had been analyzed in detail. Compared with PFSW, NTPFSW had a narrow shoulder affected zone. The stir zones (SZ) obtained by the PFSW and NTPFSW were both composed of fine equiaxed grains. The grains in the upper part of NTPFSW joint were larger in size and the number of precipitates (θ’ phase) was less. NTPFSW completely eliminated weld thinning phenomenon and the tensile properties were improved.

1. Introduction

Friction stir welding (FSW) was one of the most successful joining techniques in the 20th century [1–3]. Due to its many advantages such as high energy efficiency, low cost, environmental friendliness and high welding quality [4, 5], FSW had gained considerable scientific and technological attention in many fields, including aerospace, railway, renewable energy and automobile [6–11]. During the welding, a suitable shoulder plunge depth could provide adequate forging force and heat input [12, 13], improved the material flow in stirring zone, avoided the formation of internal defects, and finally obtained a sound FSW joint [14, 15]. However, due to the existence of plunge depth, the flash defects and burrs were inevitably formed on the weld edge. Flash defects could cause the loss of material, and the thickness of weld was thinner than that of the base material, which was called weld thinning [16, 17]. The weld thinning had many negative effects on the joint. Firstly, the integrity of external dimension of joint was destroyed. The flash defects induced by weld thinning maybe become a potential security risks during service. Secondly, the effective load bearing area was reduced due to weld thinning [16]. Kumar et al. [18] indicated that when the plunge of the rotating shoulder increased to a certain extent, weld thinning markedly increased, which easily caused joint fracture in the weak region of the weld and drastically deteriorated the mechanical properties. Thirdly, the aluminum alloy structures, such as those used in aerospace and railway, usually beard both static load and dynamic load during service. The thinning of joint can greatly reduce its fatigue properties. In addition, the stress concentration caused by thinning can greatly reduce the stress corrosion resistance of the joint. Li et al. [19] has welded 2219 aluminum alloy by non-rotational shoulder assisted friction stir welding (NRSAFSW). Although the weld thinning was eliminated by NRSAFSW, the maximum mechanical property was only 307 MPa, equivalent to 69% of the BM. However, the tensile strength of the conventional FSW (CFSW) joint obtained at the optimal welding parameter with the same base material was 346 MPa [20], which demonstrated the mechanical

properties of joints obtained by NRSAFSW were unsatisfactory. Zhang et al. [21] designed a new type of welding tool to carry out non-thinning friction stir welding (NTFSW). A concave geometrical feature was utilized to the end surface of tool shoulder and three equally spaced scrolls were machined on the concave shoulder. In such case, the weld thinning phenomenon was avoided. However, the shoulder plunge depth was only 0 mm, and thus insufficient heat input resulted in the formation of kissing bond at the joint root.

The weld thinning reduced the actual bearing area of the weld and deteriorated the dimensional accuracy of the whole joint. At the same time, the existence of depression also led to stress concentration and reduced the mechanical property and corrosion resistance of the joints. In the conventional friction stir welding (CFSW), the length of the stirring pin was a bit shorter than the thickness of workpiece [22, 23]. Therefore, a kissing bond was formed at the joint root, resulting in the deterioration of mechanical properties. Especially, under the dynamic loading conditions, the kissing bond became a crack source in the joint, and significantly reduced fatigue strength of the joint. In order to completely cancel the king bond, Hu et al [24] designed a slight longer stirring probe than the thickness of workpiece in order to accomplish tilt probe penetrating friction stir welding (PFSW), and the kissing bond at the root was successfully eliminated, but the weld thinning phenomenon was still exist.

All in all, the previous studies have indicated that the weld thinning and kissing bond are difficult to remove from the FSW joints in the same time. To break through the limitations, a non-thinning and penetrating friction stir welding (NTPFSW) is put ward, which is expected to efficiently eliminate the weld thinning phenomenon and to avoid the formation of kissing bond at the joint root in the present study. By using the same process parameters, the microstructure and mechanical properties of NTPFSW and PFSW joints were compared and analyzed, and thus the advantage of NTPFSW was revealed.

2. Experimental Material And Procedures

The base material (BM) used in this study was 5 mm-thick 2219-T6 aluminum alloy in T6 condition with the length of 300 mm and width of 80 mm, which was a type of aviation aluminum-alloy belonging to Al-Cu series. Its chemical composition was shown in Table 1, all in wt%. The tensile strength of BM was 436 MPa and the elongation was 11.2%.

Table 1
Chemical compositions (wt.%) of the base material

Cu	Mn	Fe	Ti	V	Zn	Si	Zr	Al
6.48	0.32	0.23	0.06	0.08	0.04	0.49	0.20	Bal.

In order to produce NTPFSW joints without kissing bond and weld thinning, the welding tool should be properly designed. The tool was designed to split style, which was divided into three parts, i.e. clamping part, shoulder and stirring pin. Each part was fixed by thread, and Archimedes spiral groove was machined on the concave shoulder. The spiral groove was 2 mm in width, 0.75 mm in depth and the spiral equation was $\rho = 2/\pi$, which started from the edge of shoulder central hole and anticlockwise

extended to the outer edge of the shoulder. The shoulder diameter was 24 mm and the pin length was 6 mm. The physical NTPFSW tool was displayed in Fig. 1(a)- (d). The tool tilt angle was 0.5° and the shoulder plunge depth was 0.1mm during the NPTFSW.

The contrastive analyses of an NTPFSW joint and a PFSW joint were conducted. As displayed in Fig. 2(a), a tool with a shoulder 16 mm in diameter and a pin of 6mm in length was used in PFSW. PFSW was proved superior to CFSW in mechanical properties at at the welding speed of 300 mm/min, rotation speed of 800 rpm [24]. In order to compare with NTPFSW and PFSW, both welded joints were obtained with the same process parameters at the welding speed of 300 mm/min, rotation speed of 800 rpm. In NTPFSW and PFSW, the traditional backing plate was replaced by stationary shoulder in which a blind hole of 8 mm in diameter and 4 mm in depth was machined in the stationary shoulder center, as shown in Fig. 2(b) The function of blind hole was to accommodate the penetrated part of the stirring probe because the length of probe was longer than the thickness of workpiece. Both NTPFSW and PFSW were carried out in the same welding system, as shown in Fig. 2(c).

The microstructure analysis methods mainly included Optical Microscope (OM), Electron Backscattered Diffraction (EBSD) and Transmission Electron Microscope (TEM). The OM, EBSD and TEM samples of the welds were cross-sectioned by electrical discharge machining. Different granularity abrasive papers were used to grind samples. 2.5μm and 1μm polishing paste were used for mechanical polishing and then followed by Krolls reagent (92ml distilled water + 6ml HNO_3 + 2ml HF). The macrostructure and microstructure of the joints were observed by OM (Olympus VHX-1000). The samples were prepared by Argon ion polishing and used for SUPRA55 field emission scanning electron microscope EBSD analysis.

3. Results And Discussion

3.1 Macrostructure characteristics of welded joints

Figure 3 shows the weld cross section of the PFSW and NTPFSW joints, which are obtained at the welding speed of 300 mm/min and rotation speed of 800rpm. No kissing bond and welding defects are found in the joints obtained from either welding methods. Each joint is divided into four zones, i.e. stir zone (SZ), thermal mechanically affected zone (TMAZ), heat affected zone (HAZ) and base material (BM). The SZ is divided into shoulder affected zone (SAZ) and pin affected zone (PAZ). It can be seen that the area of SAZ in PFSW is larger than that of NTPFSW. This illustrates that under the same nominal inserting depth, the extrusion effect of NTPFSW shoulder on the upper surface of the joint is reduced, and the material flow behavior is controlled.

Compared with BM, it can be clearly found in Fig. 3a that PFSW joint is depressed and there were obvious flashes on the upper surface edge of the weld. In contrast, NTPFSW joint has a flat top surface without flashes, as shown in Fig. 2b. The arc corrugation is remarkable for pfsw, whereas the upper surface is flat for ntpfsw. In the FSW process, in order to ensure that the materials have sufficient thermal plasticization and forging forming effects, the shoulder of welding tool needs to be pressed into the workpiece to a

sufficient depth. The extruded materials become the flashes of the weld and the joint shows a significant depression relative to base metal, leading to the weld thinning phenomenon. As shown in Fig. 4, the value of weld thickness ($\triangle T$) is defined as the thickness of the base material ($\triangle T_{BM}$) minus the thickness of the joint ($\triangle T_{weld}$). $\triangle T$ of the PFSW joint is -0.12mm, which is 2.4% of the base metal thickness. In comparison, $\triangle T$ of the NTPFSW joint is 0.1mm which means the thickness of NTPFSW joints is not thinner than the BM. The tool is subject to the axial reaction force from BM while it performs forging action in the FSW process. If the axial reaction force is large enough, the tool can be lifted from its original position [25, 26]. For the welding speed of 300 mm/min, the interaction force between the tool and BM is strong. The ability of axis shoulder to converge materials together is improved by the Archimedes spiral groove on the NTPFSW shoulder, hence the ntpfsw tool also is given more axial reaction force. Therefore, the upper surface of ntpfsw joint is slightly higher relative to BM. This result indicates that the weld thinning phenomenon has been completely eliminated and non-thinning friction stir welding can be achieved by NTPFSW.

3.2 Microstructure characteristics of welded joints

The EBSD inverse pole figures (IPF) of the NTPFSW joint and PFSW joint are shown in Fig. 5. The grain size decreases from upper to bottom. The SZ of joints obtained by both welding processes consists of equiaxed grains, which are mixed by a certain number of small and large grains. Therefore, The SZ of joint undergoes complete dynamic recovery and dynamic recrystallization during the friction heat generation and intense plastic deformation. The grain size of the joints decreases gradually from top to bottom. The vast majority of the grains are trended to < 111 > orientation (blue). The grain elongation in the upper part of NTPFSW joint is more obvious. Figure 5 shows the number and area fraction of grains with varied sizes. As shown in Fig. 6 (a), the average grain size in the upper part of NTPFSW joint and PFSW joint are respectively 7.86 μm and 7.26 μm. The proportion of grains with the size greater than 15 μm is significantly high in the NTPFSW joint. In Fig. 5, black lines correspond to high angle boundaries (HABs) with misorientation angles exceeding 15° and the red lines correspond to low angle boundaries (LABs) with misorientation angles ranging from 2° to 5°. Obviously, the HAB content of HABs in upper part of NTPFSW joint reaches to 75.5%, which is higher than that in PFSW joint. Compared with PFSW joint, the random distribution of grain orientation in NTPFSW joint is more obvious.

In conclusion, the diameter of ntpfsw shoulder is larger than that of pfsw and the peak temperature is higher and the high temperature residence time is longer, and the grain can fully grow. The fine equiaxed crystals in the joint are mostly surrounded by HABs, which does not contain substructures. Their growth conforms to the definition of discontinuous dynamic recrystallization [27]. The grain size of the ntpfsw and pfsw joints decreases gradually from the upper part to the lower part of joints, as commonly observed in other published literature for the FSW joints [28]. With respect to the NPTFSW joint, the magnitude of grain size change in three layers is smaller than that in PFSW. It is thus deduced that, in comparison with PFSW, the thermal effects of NTPFSW joints are obvious and the variational range of grain size is smaller along the direction of plate thickness [21].

3.3 Precipitate evolution in the SZ

Precipitates in the SZ of FSW joints are illustrated in Fig. 7. The θ' phases are indicated by the red arrow. Compared with the high-density needle-like θ' phase in the BM (Fig. 6a), the density of θ' phase in the SZ is significantly reduced because a lot of θ’ phases are dissolved into the BM under the influence of welding thermal cycle. The plate-like θ’ phase existing in SZ, as indicated by the red arrow in Fig. 7(b) and Fig. 7(c), is re-precipitated during the cooling process. Comparing Fig. 7(b) with Fig. 7(c), it can be concluded that the density and size of θ’ phase in NTPFSW joint are smaller than those of PFSW joint. This is due to the fact that the shoulder area of NTPFSW is larger than that of PFSW. With the same welding parameters, the welding thermal cycle of NTPFSW has a longer elevated temperature holding time and a slower cooling rate, which makes it possible to re-precipitate θ’ phase. PSFW produces less heat than NTPFSW, resulting in shorter elevated temperature holding time and less re-precipitate θ’ phase into BM. The size of precipitate θ’ is smaller than that in NTPFSW joint owing to the lack of time to grow up. The selected area diffraction (SAD) patterns along [0 1 1] zone axis of aluminum matrix is illustrated in Fig. 7(d). It can be seen that in addition to a set of diffraction spot of the matrix, there is another set of diffraction spot with weak brightness. After calibration, it is the diffraction pattern of θ’ phase (Al_2Cu) and the corresponding crystallographic plane index has been marked on the picture. The SAED result identifies that the light gray plate-like precipitates are θ’ phase and the re-precipitation of θ’ phase during cooling process are confirmed. Figure 8 shows the element mapping of SZ in NTPFSW joint. Clearly, apart from the re-precipitated θ’ phase, the large black phases are high melting point intermetallic, which contains Mn, Fe, Si, Zr and other elements. These elements may form precipitating phases of Al_3Zr and $Cu_2Mn_3Al_{20}$, which are also prone to appear in 2219 aluminum alloy [29, 30].

3.4 Mechanical properties of welded joints

In order to compare the joint properties, a strength factor is defined as the joint tensile strength divided by the BM tensile strength. The tensile properties of joints are shown in Fig. 9. It can be seen from Fig. 9 that the tensile strength of NTPFSW joint is 365 MPa and the strength factor is 83.7%, which is 2% higher than that of PFSW joint (355 MPa, 81.4%). Moreover, the elongation of joint is increased from 7.5–9.3%.

All in all, by means of non-thinning welding method, the tensile properties of the joint are not reduced and are slightly enhanced. From the previous section 3.1, it can be revealed that the thickness of NTPFSW weld is 0.22mm thicker than that of PFSW weld, which is 4.4% of BM thickness. The thickness increment of 4.4% can elevate the tensile strength by 10MPa. In summary, this result proves that the elimination of weld thinning produces an improvement to tensile properties of the joint.

To further clarify the effects of joint microstructure on the tensile properties, the fracture positions and surfaces of the joints were examined. As can be observed from Fig. 10a and 10b, at the welding process parameters of 800 mm/min and 300 rpm, the crack propagates from the SZ periphery of weld bottom and extends along TMAZ. The necking phenomenon can be obviously observed in ntpfsw joint (Fig. 10a). In the mass, both joints are composed of a large number of dimples and partial tearing edge, which shows a typical ductile fracture. The size of dimple in the middle of the joint is larger than that in the upper part. By comparing Fig. 10(c-e) and Fig. 10(f-h), it can be found that the number of tearing edges is

more in PFSW joint. The necking phenomenon and the number of tearing edges illustrate that the toughness of ntpfsw joint is better, which is consistent with the previous test results. As displayed in Fig. 10(c) and Fig. 10(f), the dimple size of the upper part of ntpfsw joint is smaller than that of PFSW joint. The reason for this effect is that the size of ntpfsw is large, so its linear velocity is higher at the same rotation speed. In addition, the shoulder contains Archimedes spiral groove, so the strain rate of the upper part is higher, correspondingly, the size of dimples is small [31].

4. Conclusions

(1) A novel FSW tool with large-size shoulder and Archimedes spiral groove is designed and the weld thinning phenomenon is successfully eliminated. Compared with PFSW, the weld thickness of NTPFSW increases by 4.4%.

(2) The upper part of NTPFSW joint is composed of fine equiaxed grains and the grain size is larger than that of PFSW joint as well. The variation range of grain size is smaller along the direction of plate thickness.

(3) The density of θ' phase in the SZ is significantly reduced because a lot of θ’ phase is dissolved into the BM, and the density and size of θ’ phase in the NTPFSW joint are smaller than those of PFSW joint. PFSW produces less heat than NTPFSW, and less re-precipitate θ’ phase into BM. The size of precipitate θ’ is smaller than that in NTPFSW joint owing to the lack of time to grow up.

(4) The tensile strength of NTPFSW joint is up to 365 MPa, the strength factor is 83.7% and the fracture elongation is 9.3%. Such a result proves that the elimination of weld thinning produces an improvement to tensile properties.

Declarations

Author contribution

Dongrui Li: Data curation and writing—original draft. Huijie Liu: Writing—review and editing. Siping Chen: Data curation. Shuaishuai Du: Writing—review and editing. Yanying Hu: Writing—review and editing. Xuanmo Li: Data curation. Yisong Gao: Writing—review and editing

Funding

This study was kindly supported by the National Natural Science Foundation of China (No. 52075122 and No. 51775143).

Availability of data and material

The raw/processed data required to reproduce these findings cannot be shared at this time as the data also forms part of an ongoing study.

Competing interests The authors declare no competing interests.

References

1. Rai R, De A, Bhadeshia HKDH, DebRoy T (2013) "Review: friction stir welding tools,". Sci Technol Weld Joining 16(4):325–342. doi: 10.1179/1362171811y.0000000023
2. Thomas WM, Nicholas ED (1997) "Friction stir welding for the transportation industries," (in English), *Materials & Design*, vol. 18, no. 4–6, pp. 269–273, Dec doi: 10.1016/S0261-3069(97)00062-9
3. Meng XC, Huang YX, Cao J, Shen JJ, dos Santos JF (2021) "Recent progress on control strategies for inherent issues in friction stir welding," (in English), *Progress in Materials Science*, vol. 115, Jan doi: ARTN 100706 1016/j.pmatsci.2020.100706
4. Ma ZY (2008) "Friction Stir Processing Technology: A Review,". Metall Mater Trans A 39(3):642–658. doi: 10.1007/s11661-007-9459-0
5. Threadgill PL, Leonard AJ, Shercliff HR, Withers PJ (2013) Friction stir welding of aluminium alloys,. Int Mater Rev 54(2):49–93. doi: 10.1179/174328009x411136
6. Mishra RS, Ma ZY (2005) "Friction stir welding and processing,". Mater Sci Engineering: R: Rep 50:1–2. doi: 10.1016/j.mser.2005.07.001
7. Magalhães VM, Leitão C, Rodrigues DM (2018) "Friction stir welding industrialisation and research status,". Sci Technol Weld Joining 23(5):400–409. doi: 10.1080/13621718.2017.1403110
8. Liu HJ, Li JQ, Duan WJ (2012) "Friction stir welding characteristics of 2219-T6 aluminum alloy assisted by external non-rotational shoulder,". Int J Adv Manuf Technol 64:9–12. doi: 10.1007/s00170-012-4132-1
9. Zhang ZH, Li WY, Feng Y, Li JL, Chao YJ "Global anisotropic response of friction stir welded 2024 aluminum sheets," (in English), *Acta Materialia*, vol. 92, pp. 117–125, Jun 15 2015, doi: 10.1016/j.actamat.2015.03.054
10. Zhou C, Yang X, Luan G (2005) "Fatigue properties of friction stir welds in Al 5083 alloy," *Scripta Materialia*, vol. 53, no. 10, pp. 1187–1191, doi: 10.1016/j.scriptamat.2005.07.016
11. Lombard H, Hattingh DG, Steuwer A, James MN (2008) "Optimising FSW process parameters to minimise defects and maximise fatigue life in 5083-H321 aluminium alloy,". Eng Fract Mech 75:3–4. doi: 10.1016/j.engfracmech.2007.01.026
12. Arbegast WJ (2008) "A flow-partitioned deformation zone model for defect formation during friction stir welding,". Scripta Mater 58(5):372–376. doi: 10.1016/j.scriptamat.2007.10.031
13. Gemme F, Verreman Y, Dubourg L, Wanjara P (2011) Effect of welding parameters on microstructure and mechanical properties of AA7075-T6 friction stir welded joints,. Fatigue & Fracture of Engineering Materials & Structures 34(11):877–886. doi: 10.1111/j.1460-2695.2011.01580.x
14. Liu HJ, Hu YY, Dou C, Sekulic DP (Jan 2017) An effect of the rotation speed on microstructure and mechanical properties of the friction stir welded 2060-T8 Al-Li alloy," (in English). Mater Charact 123:9–19. doi: 10.1016/j.matchar.2016.11.011

15. Doude HR, Schneider JA, Nunes AC (2014) Influence of the Tool Shoulder Contact Conditions on the Material Flow During Friction Stir Welding,. Metall Mater Trans A 45(10):4411–4422. doi: 10.1007/s11661-014-2384-0
16. Sattari S, Bisadi H, Sajed M (2012) Mechanical Properties and Temperature Distributions of Thin Friction Stir Welded Sheets of AA5083,. Int J Mech Appl 2(1):1–6. doi: 10.5923/j.mechanics.20120201.01
17. Huang YX, Wan L, Lv SX, Zhang Z, Liu HJ (2012) New technique ofin siturolling friction stir welding,. Sci Technol Weld Joining 17(8):636–642. doi: 10.1179/1362171812y.0000000056
18. Kumar M, Kailas SV, Narayanan RG (2013) Influence of external weld flash on the in-plane plane-strain formability of friction stir welded sheets,. J Strain Anal Eng Des 48(6):376–385. doi: 10.1177/0309324713488884
19. Li JQ, Liu HJ (2013) "Effects of tool rotation speed on microstructures and mechanical properties of AA2219-T6 welded by the external non-rotational shoulder assisted friction stir welding," (in English), *Materials & Design*, vol. 43, pp. 299–306, Jan doi: 10.1016/j.matdes.2012.07.011
20. Hu YY, Liu HJ, Fujii H (Sep 2019) "Improving the mechanical properties of 2219-T6 aluminum alloy joints by ultrasonic vibrations during friction stir welding,". (in English) Journal of Materials Processing Technology 271:75–84. doi: 10.1016/j.jmatprotec.2019.03.013
21. Zhang HJ et al "Microstructure-property characteristics of a novel non-weld-thinning friction stir welding process of aluminum alloys," (in English), *Materials & Design*, vol. 86, pp. 379–387, Dec 5 2015, doi: 10.1016/j.matdes.2015.06.106
22. Khodaverdizadeh H, Heidarzadeh A, Saeid T (2013) "Effect of tool pin profile on microstructure and mechanical properties of friction stir welded pure copper joints,". Mater Design 45:265–270. doi: 10.1016/j.matdes.2012.09.010
23. Marzbanrad J, Akbari M, Asadi P, Safaee S (2014) Characterization of the Influence of Tool Pin Profile on Microstructural and Mechanical Properties of Friction Stir Welding,. Metall Mater Trans B 45(5):1887–1894. doi: 10.1007/s11663-014-0089-9
24. Hu YY, Liu HJ, Li S, Du SS, Sekulic DP "Improving mechanical properties of a joint through tilt probe penetrating friction stir welding," (in English), *Materials Science and Engineering a-Structural Materials Properties Microstructure and Processing*, vol. 731, pp. 107–118, Jul 25 2018, doi: 10.1016/j.msea.2018.06.036
25. Atharifar H, Lin DC, Kovacevic R (2009) "Numerical and Experimental Investigations on the Loads Carried by the Tool During Friction Stir Welding," (in English), *Journal of Materials Engineering and Performance*, vol. 18, no. 4, pp. 339–350, Jun doi: 10.1007/s11665-008-9298-1
26. Trimble D, Monaghan J, O'Donnell GE (2012) Force generation during friction stir welding of AA2024-T3," (in English). Cirp Ann-Manuf Techn 61(1):9–12. doi: 10.1016/j.cirp.2012.03.024
27. Suhuddin UFHR, Mironov S, Sato YS, Kokawa H "Grain structure and texture evolution during friction stir welding of thin 6016 aluminum alloy sheets," (in English), *Materials Science and Engineering a-*

Structural Materials Properties Microstructure and Processing, vol. 527, no. 7–8, pp. 1962–1969, Mar 25 2010, doi: 10.1016/j.msea.2009.11.029

28. Xu WF, Liu JH, Luan GH, Dong CL (2009) "Temperature evolution, microstructure and mechanical properties of friction stir welded thick 2219-O aluminum alloy joints," (in English), *Materials & Design*, vol. 30, no. 6, pp. 1886–1893, Jun doi: 10.1016/j.matdes.2008.09.021
29. Tsivoulas D, Robson JD (2015) Heterogeneous Zr solute segregation and Al3Zr dispersoid distributions in Al–Cu–Li alloys,. Acta Mater 93:73–86. doi: 10.1016/j.actamat.2015.03.057
30. Tsivoulas D, Prangnell PB (2014) "Comparison of the Effect of Individual and Combined Zr and Mn Additions on the Fracture Behavior of Al-Cu-Li Alloy AA2198 Rolled Sheet,". Metall Mater Trans A 45(3):1338–1351. doi: 10.1007/s11661-013-2103-2
31. Frigaard O, Grong O, Midling OT (2001) "A process model for friction stir welding of age hardening aluminum alloys," (in English), *Metall Mater Trans A*, vol. 32, no. 5, pp. 1189–1200, May doi: DOI 10.1007/s11661-001-0128-4

Figures

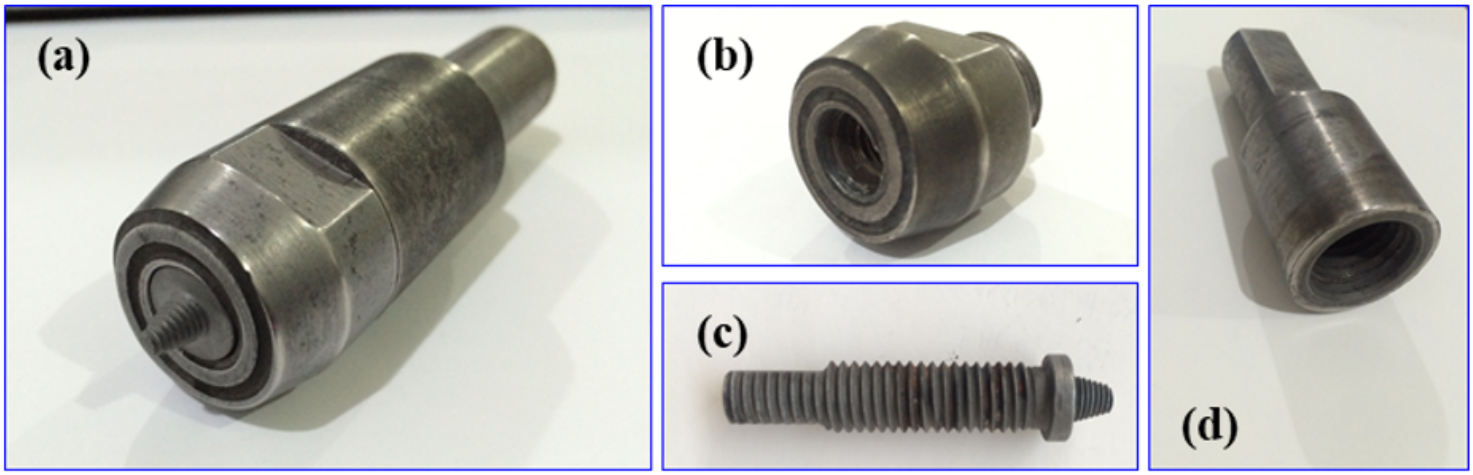

Figure 1

NTPFSW tool (a) integrity of tool, (b) shoulder with Archimedes spiral groove, (c) stirring pin, (d) clamping part

Figure 2

PFSW tool and welding system: (a) integrity of tool, (b) stationary shoulder, (c) welding system

Figure 3

Cross-section macrostructure of the joint (a) PFSW (b) NTPFSW

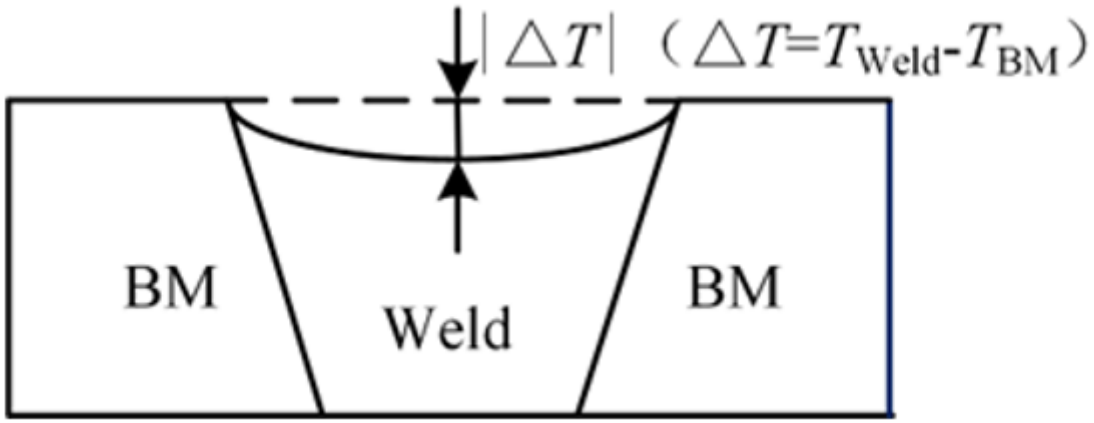

Figure 4

Schematic diagram of weld thinning △T

Figure 5

EBSD images of the different parts of SZ: (a-c) upper, middle and lower parts of NTPFSW joint; (d-e) upper, middle and lower parts of PFSW joint

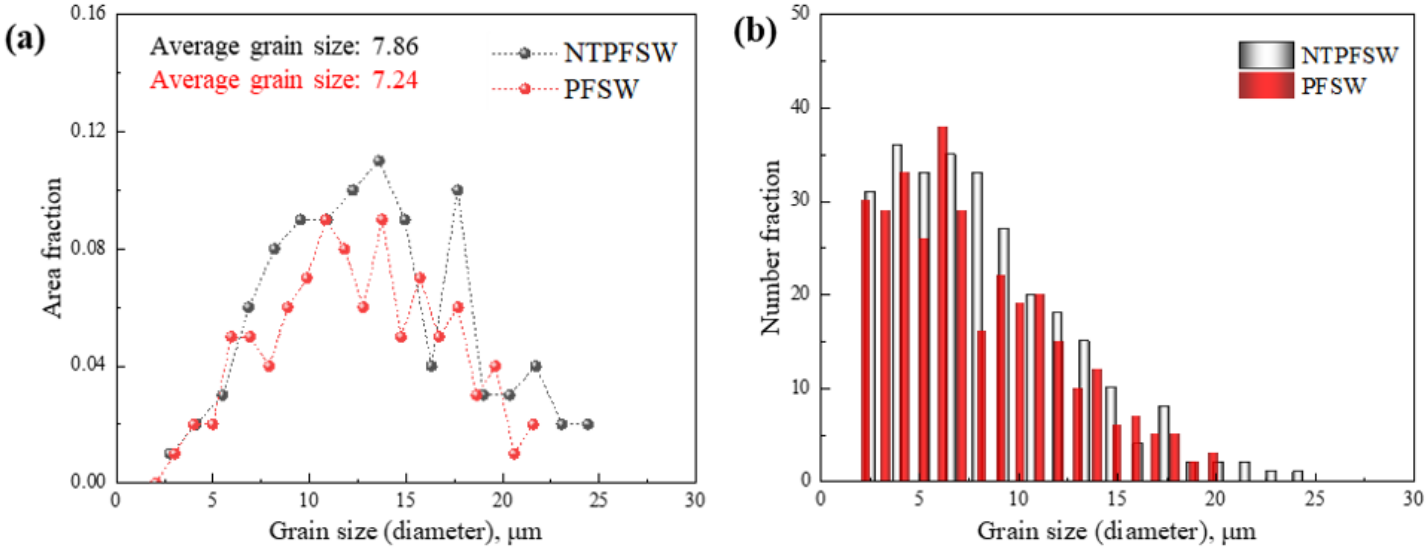

Figure 6

Change of area and number fraction of grains with grain sizes: (a) Area fraction; (b) Number fraction

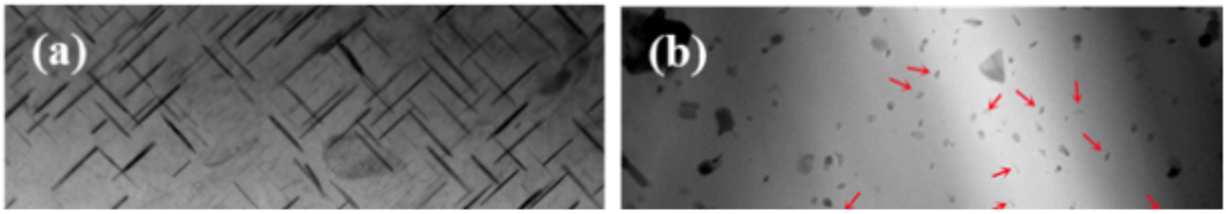

Figure 7

Bright field images of the precipitates in the SZ: (a) BM, (b) PFSW joint, (c) NTPFSW joint, (d) SAED patterns of the NTPFSW joints at the zone axis

Figure 8

Element mappings of the SZ obtained by NTPFSW

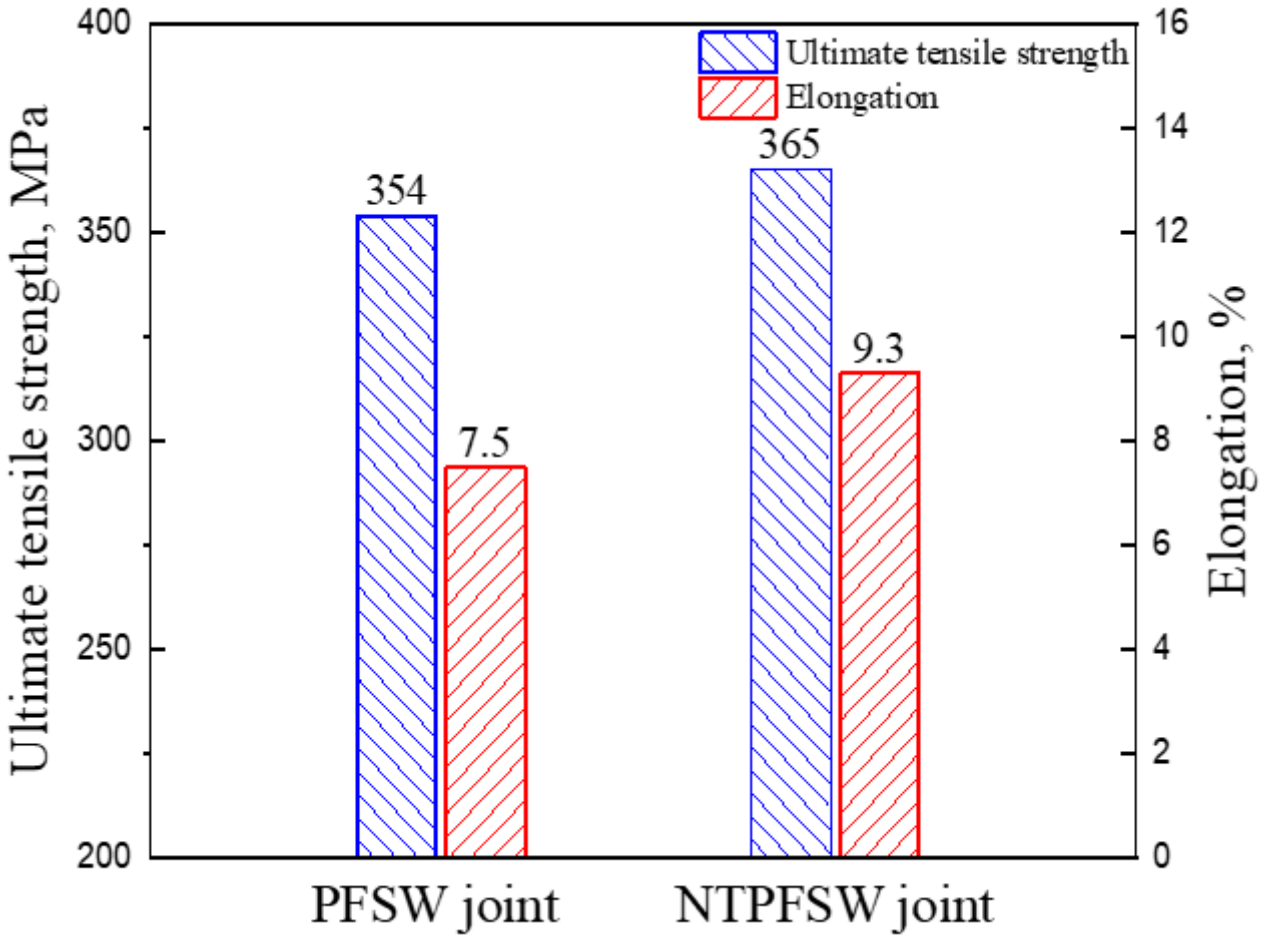

Figure 9

Tensile strength and elongation of the joints

Figure 10

Fracture behavior of the joints. (a) and (b) Fracture positions of NTPFSW and PFSW joints,

(c)–(e) Fracture morphologies of NTPFSW, (f)–(h) Fracture morphologies of PFSW